Definition, Implementation, and Evaluation of a Novel Spiral-Sampling Technique

Vivek H. Sanandiya, Scott T. McBride
NSI-MI Technologies
Suwanee, GA, 30024 USA
vsanandiya@nsi-mi.com
smcbride@nsi-mi.com

***Abstract*— Building on the theory of spiral near-field acquisitions, the authors present a novel spiral acquisition implemented in a spherical near-field (SNF) chamber for a large automotive application. This new spiral permits the relaxation of certain restrictions associated with the standard spiral. Specifically, it allows us to eliminate extra or redundant rings beyond the poles, allows for greater control of the angular velocity ratio (i.e. gear ratio) between the theta and phi physical positioning axes, and does not require that the theta axis retrace between acquisitions.**

In this paper, we describe the new spiral's motivations, implementation, advantages, and measurement results. We first discuss the new spiral sampling, its mathematical definition, and its comparison to a standard spiral. Next, we describe the practical considerations and implementation of the coordinated motion between theta and phi for spiral sampling over a spherical surface. Next, we present the results showing good pattern agreement between conventional SNF and the new spiral method. We also discuss the reductions in near-field acquisition time and total test time that were achieved using the new spiral.

Keywords—spherical near-field, spiral sampling

I. INTRODUCTION

The theory of sparsely sampling the near field (NF) of an antenna under test (AUT) has been available for over 30 years. It was introduced to the test and measurement community in 1987 [1] with the development of a general theory on the spatial bandwidth of a signal emanating from a generic geometric boundary. Many papers have been written building on this general framework including several papers (e.g. [2]-[5]) on a method for acquiring data in a spiral configuration.

Prior research has focused primarily on the number of samples required to accurately reconstruct the far-field patterns of the AUT. These publications demonstrate potential improvement in acquisition time but stop short of demonstrating such utility in a practical system. In 2017, the authors described some of the practical limitations associated with implementing the spiral theory in an SNF system [6]. In this study, they also implemented a simple spiral in a roll-over-azimuth SNF range that began to address some of the practical considerations discussed.

Some of the practical limitations of the standard spiral discussed in [6] include the following:

1. The spiral has a non-constant pitch, so coordination between the motion of two axes must vary the relative angular velocities (gear ratio) of the two physical axes
2. Electrically large AUTs lead to a very large gear ratio, which causes one of the axes to move very slowly, potentially causing problems with stiction
3. Optimal spacing in ϕ is dramatically reduced near the poles, creating a discontinuity in the velocity profile
4. Additional rings are required beyond the poles, leading to a discontinuity in the velocity profile of the theta axis when implemented in an arch system

In this paper, we report results from an implementation of a new multi-pronged spiral in an arch (θ) and turntable (ϕ) based SNF system. With the presence of the turntable, this becomes a hemispherical scanning system. The new spiral design addresses the problems of large gear ratios (issue #2 above) and eliminates the need for additional rings beyond the poles (issue #4). Like the work in [6], this paper assumes a spherical AUT bounding surface with conventional phi spacing, eliminating the other two issues (#1 and #3) for this test at the cost of a small increase in acquisition time.

The remainder of this paper is organized as follows. In Section II, we describe the multi-pronged spiral and its advantages in addressing some of the limitations described above. In Section III, we discuss its implementation in the arch SNF system and present samples of far-field (FF) pattern data showing good agreement with a conventional SNF measurement. In Section IV, we discuss acquisition and test time for both conventional SNF and the new spiral. Conclusions and future work are discussed in Section V.

II. THE MULTI-PRONGED SPIRAL

Motivated by the limitations discussed above, including the need for additional rings around the pole (which eats away at any advantage the spiral gives us in reducing acquisition time) and the gear ratio (which has the potential to degrade the quality of our measurements), we define the following spiral:

Given a number of branches, N, let the n^{th} branch be defined as:

$$N_\theta = \frac{\theta_{max}}{d\phi} + 1 \tag{1}$$

$$\phi_n(N) = \left(0 : d\phi : \frac{360 * N_\theta}{N}\right) + \frac{360^o\,(n-1)}{N} \tag{2}$$

$$\theta(N) = \left(N d\theta \frac{\phi_0(N)}{360}\right) \tag{3}$$

where $d\theta$=$d\phi$ is the angular step size computed for a standard SNF scan, i.e.

$$d\phi \leq \frac{180^o}{ka + 10} \tag{4}$$

where k is the wavenumber, a is the radius of the minimum sphere, and $d\phi$ is chosen as the largest value that meets the constraint above while also allowing for an integer number of samples around a great circle on the sphere.

This definition of the multi-pronged spiral currently restricts us to equal angular steps, but it can be modified to accommodate non-uniform pitch. In addition to the spiral, in order to sufficiently cover the NF surface for a hemispherical scan, we also acquire a single cut along the equator. An example illustration of a six-pronged spiral (blue dots) and equatorial cut (red circles) is depicted in Figure 1. where $d\phi = 10^o$.

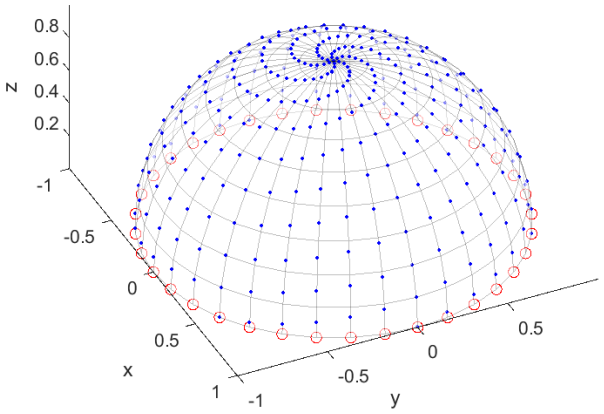

Figure 1. Example of a six-pronged hemispherical spiral with equatorial cut.

With this new spiral, when N is an even number, we can interpolate across the pole by stitching two of the prongs together. This gives us sufficient sample density at the pole and a set of points in a linear dimension over which we can interpolate, thus eliminating the need for extra rings around the pole. For comparison, and to illustrate the extra rings, Figure 2. shows a standard spiral with two extra rings around the pole (red dots). Note, however, that the actual number of rings required may be much larger. Each of these extra samples adds to the total acquisition time, eating away at the major advantage offered by this sparse sampling.

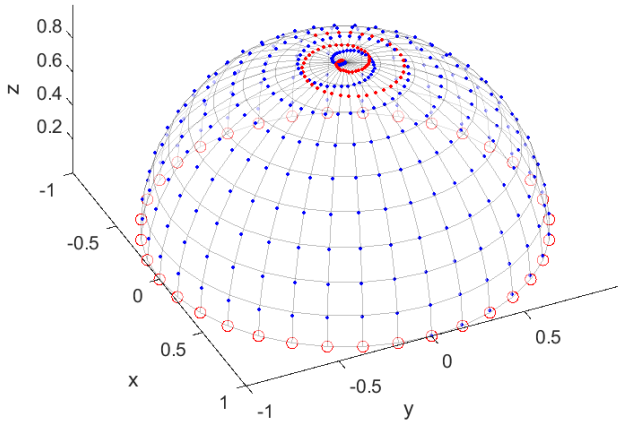

Figure 2. Example of a standard hemispherical spiral with two extra rings at the north pole and an equatorial cut.

In addition to eliminating the extra rings, the use of an even number of prongs allows us to end our acquisition at the start position, improving our efficiency in taking multiple data sets when using a large arch.

Another major advantage of the technique is the flexibility it offers in controlling the gear ratio. With a larger number of prongs, we have a smaller pitch, which reduces the required gear ratio. If stiction in the theta axis becomes a problem, then, we can simply break the spiral into a larger number of prongs to allow the theta axis to speed up.

One potential disadvantage of this multi-prong spiral is the finite number of continuous derivatives in the contour across the pole. Bucci et al [7] correctly state that the bandlimited interpolation will work best when that contour is an analytical function (i.e. infinitely differentiable). Figure 3. shows that the acceleration of probe y is computable, but not differentiable, at the pole. If this has an impact on fidelity, it will be in the interpolation vs. theta near the pole.

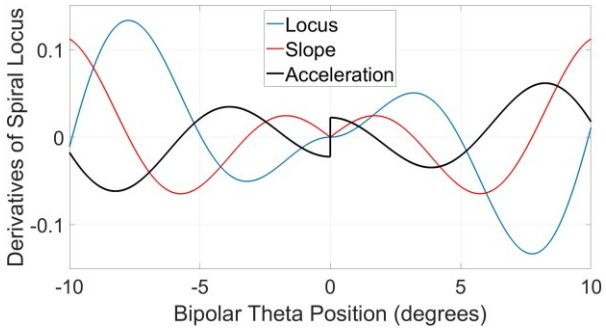

Figure 3. $\delta^n y/\delta\theta^n$ near pole

III. Implementation of the Spiral

In this section we describe the measurement setup and near-field data acquisition of the new spiral vs. the regular grid.

A. Measurement Setup

Measurements were made in a spherical near-field (SNF) chamber designed for Automotive measurements. The chamber had arch (θ) and turntable (ϕ) based SNF system, as shown in Figure 4. . The origin of the coordinate system is at the center of the turntable surface.

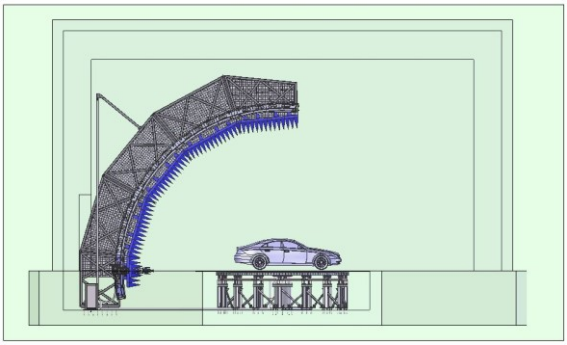

Figure 4. SNF Chamber for Automotive Measurements

A standard gain horn (SGH) operating from 3.95 GHz to 5.85 GHz was selected as the test article. The SGH was mounted on the turntable, pointing up at the pole. A dual-ridged horn was used as a probe and mounted on the arch. The SGH aperture size is 0.224 m x 0.168 m (8.8 in. x 6.6 in.) and the horn was mounted with its aperture at 0.9 m height from the turntable surface, yielding a minimum sphere diameter of 2 m. An angular step size of 1.25 degrees was used to ensure a sufficient number of spherical wave modes are captured.

B. Near-Field Measurement

Two sets of near-field data were collected. A conventional raster was collected over the upper hemisphere on a regular grid to compare its transformed data to the far-field patterns generated from the spiral data.

The measurement for the spiral case was performed using a 2-prong spiral as defined previously, with uniform phi spacing. In addition, a single equatorial scan with equal spacing in phi was collected. The total sample positions collected for the spiral is the same as the raster scan on regular grid. When running at full speed of the positioners, the uniform phi spacing is not a disadvantage because enlarging the phi increment would merely increase receiver-idle time and eliminate any benefits of the effective oversampling. A non-uniform theta spacing does not give us much advantage in this geometry but introduces significantly more complexity.

The probe was positioned on the new spiral grid by implementing a coordinated motion between phi and theta axes. A script was developed in the NSI-MI Arena measurement software to calculate motion parameters and the optimum number of spiral prongs based on the record increment, minimum theta axis speed, and gear ratio between phi and theta axes. The computed motion parameters are used to configure the NSI-MI ELE-IPC position controller for coordinated motion, which generates a motion profile for phi and theta axes to scan along the new spiral geometry.

The collected near-field data in the new multi-prong spiral geometry are then interpolated along theta to the conventional regular grid. Once on the conventional grid, the conventional SNF transform is used to produce the far field. The principal-plane cuts of the far-field patterns from spiral- and regular- grid measurements are plotted and compared in Figures 5-8. The far-field patterns are overlaid after normalizing the peak to zero, and the equivalent stray-signal level (ESSL) is shown by subtracting the voltage magnitudes of the patterns. This example shows good agreement between the conventional-grid measurement and the new spiral. Note that the ESSL at the peak (at the pole in the near-field geometry) is very low, suggesting that the limited number of continuous derivatives in the multi-prong profile was not a significant error contributor.

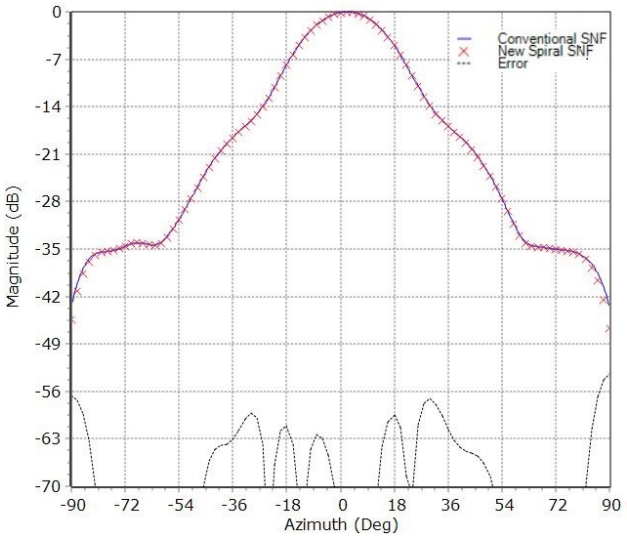

Figure 5. Co-pol H-plane far-field patterns

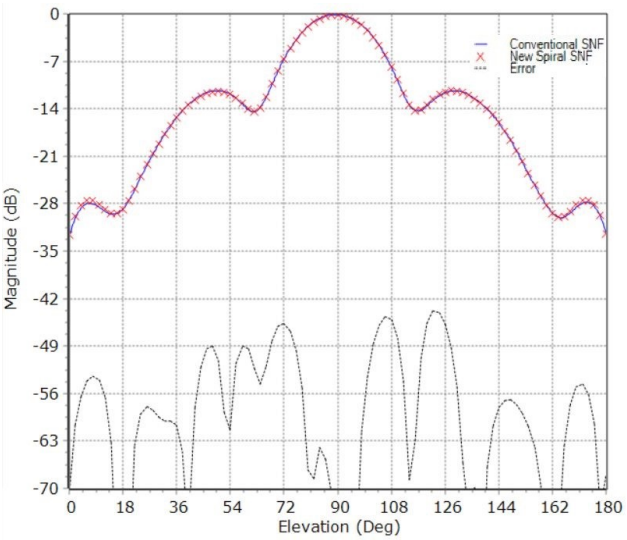

Figure 6. Co-pol E-plane far-field patterns

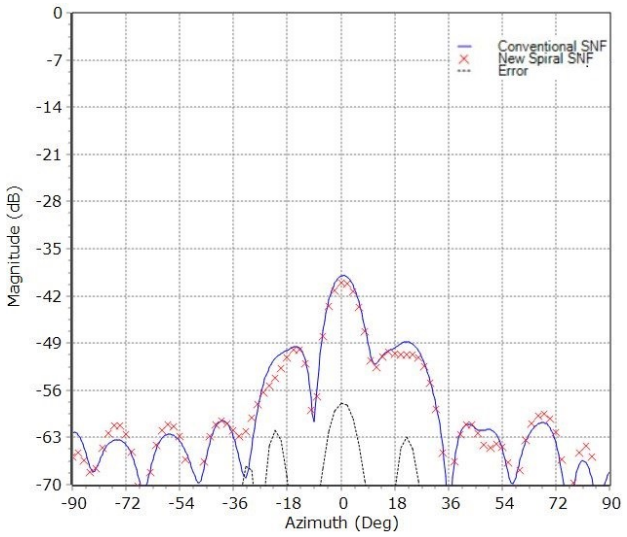

Figure 7. Cross-pol H-plane far-field patterns

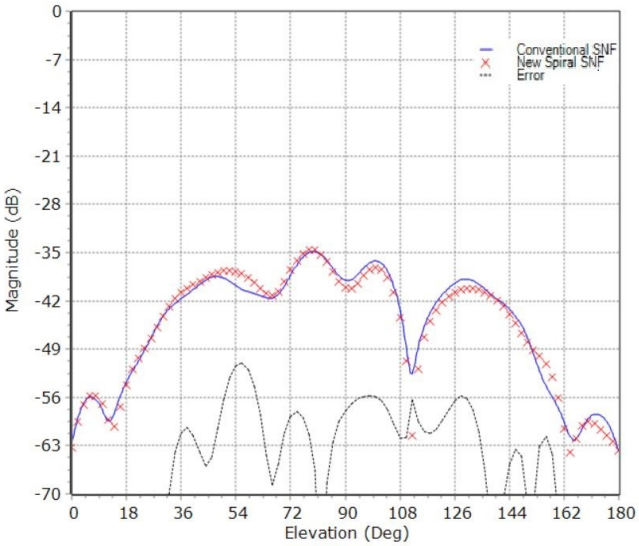

Figure 8. Cross-pol E-plane far-field patterns

Further analyses of far-field pattern parameters for the new spiral scan vs. conventional regular grid scans show good agreement for directivity and 3dB beam width, as shown in Table 1.

TABLE I. CONVENTIONAL SNF VS NEW SPIRAL RESULT

Frequency (GHz)	Directivity (dB)		3dB Beam Width, H-Plane (Deg)		3dB Beam Width, E-Plane (Deg)	
	Conventional	*Spiral*	*Conventional*	*Spiral*	*Conventional*	*Spiral*
3.95	17.24	17.25	25.11	25.08	24.24	24.30
4.43	18.12	18.15	23.28	23.13	21.50	21.49
4.90	18.67	18.69	21.28	21.30	20.21	20.08
5.38	19.13	19.15	19.85	19.77	18.87	18.83
5.85	19.49	19.52	19.05	19.00	17.20	17.15

IV. ACQUISITION- AND TEST-TIME COMPARISONS

One of the advantages offered by the new spiral sampling over the regular grid measurement is reduction in measurement time. While the number of samples collected remain the same for both, the implementation of the new spiral allows for continuous scans in phi and theta, saving the time it takes the theta axis to step in regular grid raster scans. Because in this application the turntable was rotating at its maximum speed throughout, there would have been no time savings with sparse phi sampling.

Time taken for a raster measurement on the regular grid with uniform spacing in theta and phi can be written as:

$$T_R = ((T_s + T_{step}) * (N_t\text{-}1) + T_s) + T_e + T_d \quad (5)$$

where

T_R = Total time for regular sampling

T_s = Time for one scan in phi

T_{step} = Time taken to step the theta

N_t = Total number of theta increments

T_e = Instrument initialization time, measurement start

T_d = Time for post-processing and transform

Similarly, for a measurement performed using the new spiral we can write:

$$T_{NS} = ((T_{s\_S} + T_{step\_S}) *(N_p\text{-}1) + T_{s\_S}) + T_{e\_S} + T_{d\_S} + T_{e\_S} \quad (6)$$

where

T_{NS} = Total time for new spiral sampling

T_{s_S} = Time for one prong scan

T_{step_S} = Time taken to step between prongs

N_p = Total number of Prongs

T_{e_S} = Instrument initialization at measurement start

T_{d_S} = Time for post-processing and transform

T_{e_S} = Time required for equatorial scan setup

In practice, time to initialize equipment at the start of the measurement and post-processing the data is found to be similar in both cases, and it is small in absolute terms when compared to the measurement acquisition time. Also, because both measurements are performed with uniform and same spacing in theta and phi, the total time spent acquiring data is the same. That leaves the time required to step in theta for a regular grid measurement and between prongs for the new spiral sampling measurement.

Some basic conclusions can be derived by comparing the overhead time in both cases.

- Spiral sampling will have more time advantage as the sampling increment size decreases
- Scanning at higher speed in phi favors spiral sampling, because it increases the overhead ratio of time taken to step theta to actual scan time. Also, it allows for a better gear ratio between the phi and theta axes in new spiral measurements.
- The advantage of the new spiral sampling decreases with an increase in number of prongs. This again is limited by the gear ratio.

For a given system the parameters defined in equation (5) and (6) will depend on more fundamental parameters like time taken at each sample point, which is in turn dependent on number of frequencies and beams measured, receiver IFBW and overhead. It will also depend on the total number of samples, defined by the minimum sphere size and highest frequency.

Figures 9-11 show the time comparison between a regular grid measurement and new spiral measurement for a SNF acquisition with the following parameters: Max phi scan speed of 18 deg/sec, slowest theta speed of 0.01 deg/sec, nominal increment size of 1.25 deg, and nominal number of spiral prongs of 2.

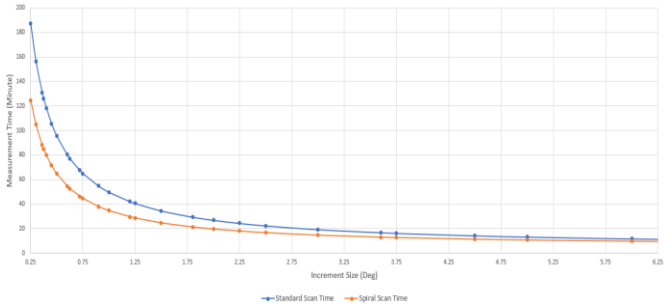

Figure 9. Measurement Time vs Increment Size

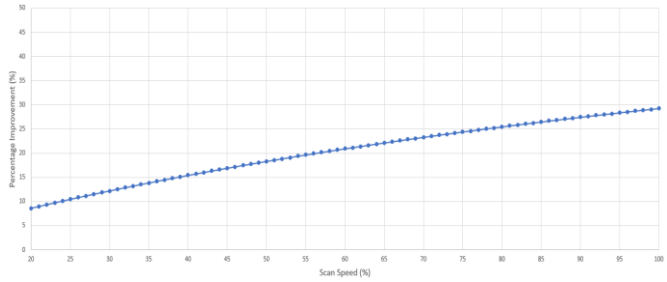

Figure 10. Time Improvement vs Phi Scan Speed

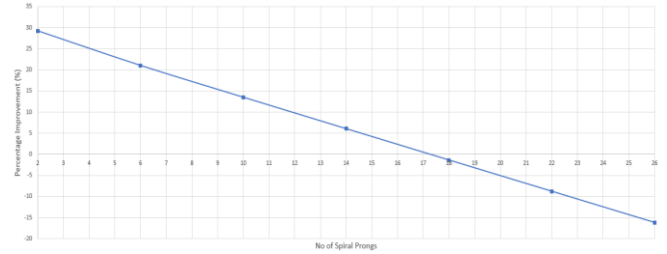

Figure 11. Time Improvent vs No. of Spiral Prongs

V. Conclusion

A novel multi-prong spiral is proposed and implemented. The new spiral allows interpolation across the pole, thus eliminating the need for extra rings at the pole. With an even number of prongs, it also allows us to end our acquisition at the start position. It also provides flexibility in controlling the gear ratio, if stiction in the theta axis becomes a problem, since we can simply break the spiral into a larger number of prongs to allow the theta axis to speed up.

Results from implementation are presented in the form of far-field pattern comparisons showing good agreement with patterns obtained from a regular grid of near-field samples. Test time comparison identifying different dependencies is shown between new spiral and regular grid measurement. The comparison shows more than 30% increase in throughput for certain measurements.

The spiral is initially implemented for uniform sampling in theta and phi. Future work will include implementing non-uniform phi and theta steps for minimizing the number of samples. Other geometries including PNF and CNF will also be explored.

Acknowledgement

The authors wish to thank Brett Walkenhorst and David Howard for their help with development and implementation of this novel spiral-sampling technique.

References

[1] O.M. Bucci, G. Franceschetti, "On the spatial bandwidth of scattered fields," *IEEE Trans. Antennas Propagat.*, vol. AP-35, pp. 1445-1455, Dec 1987.

[2] O.M. Bucci, C. Gennarelli, G. Riccio, C. Savarese, "Probe compensated NF-FF transformation with helicoidal scanning," *Journal of Electromagnetic Waves and Applications*, vol. 14, pp. 531-549, 2000.

[3] O.M. Bucci, F.D'Agostino, C. Gennarelli, G. Riccio, C. Savarese, "Probe compensated FF reconstruction by NF planar spiral scanning," *IEE Proc. Microwave Antennas and Propagation*, vol. 149, pp. 119-123, Apr 2002.

[4] O.M. Bucci, F. D'Agostino, C. Gennarelli, G. Riccio, C. Savarese, "NF-FF transformation with spherical spiral scanning," *IEEE Antennas Wireless Propagation Letters*, vol. 2, pp. 263-266, 2003.

[5] F. D'Agostino, C. Gennarelli, G. Riccio, C. Savarese, "Theoretical foundations of near-field-far-field transformations with spiral scannings," *Progress in Electromagnetics Research (PIER)*, vol. 61, pp. 193-214, 2006.

[6] B.T. Walkenhorst, S.T. McBride, "Acquisition, reconstruction, and transformation of a spiral near-field scan," *Antenna Measurement Techniques Association (AMTA) Symposium*, Oct 2017.

[7] O.M. Bucci, C. Gennarelli, C. Savarese, "Representation of electromagnetic fields over arbitrary surfaces by a finite and nonredundant number of samples," *IEEE Trans. Antennas Propagat.*, vol. 46, No. 3, pp. 351-359, Mar1998.